Angular-dependent embedded atom method potential for atomistic simulations of metal-covalent systems

Avinash M. Dongare,[1] Matthew Neurock,[2] and Leonid V. Zhigilei[1,*]
[1]*Department of Materials Science and Engineering, University of Virginia, 395 McCormick Road, P.O. Box 400745, Charlottesville, Virginia 22904-4745, USA*
[2]*Department of Chemical Engineering, University of Virginia, 102 Engineers' Way, P.O. Box 400741, Charlottesville, Virginia 22904-4741, USA*
(Received 16 June 2009; published 12 November 2009)

A computationally efficient interatomic potential is developed for the description of interatomic interactions in multicomponent systems composed of metals, Si and Ge. The potential is based on reformulation of the embedded atom method (EAM) potential for metals and Stillinger-Weber (SW) potential commonly used for Si and Ge in a compatible functional form. The potential incorporates a description of the angular dependence of interatomic interactions into the framework of the EAM potential and, therefore, is dubbed angular-dependent EAM (A-EAM) potential. The A-EAM potential retains the properties of the pure components predicted by the original EAM and SW potentials, thus limiting the scope of potential parameterization to only the cross interactions among the components. The ability of the potential to provide an adequate description of binary systems with mixed type of bonding is illustrated for Au-Si/Ge system, with the parameters for Au-Si and Au-Ge interactions determined based on the results of density-functional theory calculations performed for several representative bulk structures and small clusters. To test the performance of the A-EAM potential at finite temperatures, the values of the enthalpy of mixing of liquid Au-Si and Au-Ge alloys, as well as the equilibrium lines on the Au-Si phase diagram are evaluated and compared with experimental data. The calculation of the phase diagram is based on the values of the excess chemical potential difference between Au and Si, evaluated in a series of semi-grand canonical ensemble Monte Carlo simulations performed for different temperatures and alloy compositions. The potential is shown to provide an adequate semiquantitative description of the thermodynamic properties of the alloy at different temperatures and in the whole range of compositions, thus showing a considerable promise for large-scale atomistic simulations of metal-Si/Ge systems.

DOI: 10.1103/PhysRevB.80.184106 PACS number(s): 34.20.Cf, 61.50.Lt, 02.70.Ns, 71.15.Nc

I. INTRODUCTION

The ability of classical molecular dynamics (MD) and Monte Carlo (MC) atomistic simulation techniques to provide quantitative information on the atomic-level processes responsible for the behavior and properties of real materials and devices is, in a big part, defined by the availability of accurate and computationally efficient interatomic potentials. Over the last several decades, a broad variety of empirical and semiempirical potentials have been suggested in literature. The application of most of the proposed potentials, however, has been limited to the initial studies, with only a relatively small fraction of the potentials exhibiting a combination of transferability, computational efficiency, simplicity of implementation, and accuracy in describing various properties of materials, sufficient to ensure their broad use in simulations performed by different research groups. The embedded atom method (EAM) (Refs. 1–3) is one example of a highly successful approach as it has established the framework for a group of potentials that are used in the majority of current simulations of metals and metallic alloys. Popular potentials for covalently bonded systems include Stillinger-Weber (SW) potential[4,5] for Si and Ge, Tersoff potential[6,7] for Si and C, as well as Brenner potential[8,9] for hydrocarbon systems.

The extension of the empirical potentials to alloys consisting of components with the same type of interatomic bonding (and described by the same type of interatomic potential) is relatively straightforward, with several alloy models (schemes for the description of cross interactions between the components) developed for metals[10–14] and covalent systems.[15,16] The design of interatomic potentials capable of an adequate description of multicomponent systems with mixed types of atomic bonding, however, is a more challenging task that has to be addressed to enable atomic-scale modeling of a range of practically important systems. Computationally efficient and accurate description of systems with mixed metallic-covalent bonding, in particular, is highly desirable for investigation of interfacial properties in microelectronic devices and interconnects, as well as structural analysis of various crystalline and amorphous phases present in these systems.

The modified EAM (MEAM) potential[17] by Baskes includes parameterization for many cubic metals, as well as Si, Ge, C, H, N, and O. The potential, therefore, can be adopted for modeling of systems with mixed type of bonding, such as Mo-Si,[18] Au-Si,[19] Al-Si,[20] Ni-Si,[21] and Au-Si-O.[22] The many-body angular screening function which is used to limit the interaction range in MEAM, however, makes this potential computationally rather expensive. Moreover, the properties of both pure components and mixtures predicted by the MEAM potential have to be verified for each system of interest. For Si, for example, the short-range MEAM potential is found to be inferior compared to the SW potential in the description of the diffusion paths and activation energies of an adatom on a 2×1 reconstructed Si (001) surface[23,24] and

to exhibit a poor performance in simulations of ion sputtering of Si targets.[25] An adjustment of the parameters of the MEAM potential, therefore, is often required in order to achieve an adequate description of pure components.[25]

An attractive alternative to the design of new alloy potentials with original functional forms can be provided by the combination of well-established and thoroughly tested potentials developed for pure components within a unified approach. Despite the apparent distinctions between the functional forms and underlying physical arguments used in the description of interatomic bonding in metallic and covalent systems, there have been a number of studies that suggest that a unified approach is feasible. In particular, a description of Pt-C system with an analytical potential that, for pure components, reduces to the bond-order Brenner potential for C and an EAM-like potential for Pt has been discussed by Albe *et al.*[26] The connections between the EAM formalism and the bond-order scheme of the Tersoff potential have been discussed by Brenner,[27] whereas the relationship between the SW and MEAM potentials has been discussed by Thijsse,[28] who shows that the two potentials can be reformulated into compatible functional forms.

In this work, the idea of developing a unified interatomic potential for systems with mixed type of bonding is extended to combine the EAM potential for metals with the SW potential commonly used in simulations of Si and Ge. The combined angular-dependent EAM (A-EAM) potential incorporates a description of the angular dependence of the interatomic interactions into the framework of the EAM potential, making it compatible with the SW potential. The A-EAM potential retains all the properties of the pure components as predicted by the original SW and EAM potentials, thus eliminating the need for extensive testing and limiting the scope of the potential parameterization to cross interaction between the components. The reformulation of the EAM and SW potentials leading to the development of the unified A-EAM potential is described in Sec. II. An example of the parameterization of the cross interaction in the A-EAM potential is given for Au-Si and Au-Ge systems in Sec. III. Similarly to the approach adopted in parameterization of the MEAM potential,[19] the functional form and parameters of cross interactions in the A-EAM potential are chosen based on the results of a series of density-functional theory (DFT) calculations performed for several representative Au-Si/Ge bulk structures and small clusters. The enthalpies of mixing of Au-Si and Au-Ge liquid alloys, as well as the equilibrium lines on the phase diagram of Au-Si, predicted by the A-EAM potential are presented and related to the experimental data in Secs. IV and V. The performance of the potential in describing structural and thermodynamic properties of metal-Si/Ge alloys and perspectives for future extension of the developed methodology to other systems are briefly discussed in Sec. VI.

II. ANGULAR-DEPENDENT EMBEDDED ATOM METHOD POTENTIAL

The EAM is currently the method of choice for the description of interatomic interactions in classical atomistic simulations of metals, whereas the majority of simulations for Si and Ge are performed with either SW or Tersoff potentials. A unified alloy potential based on a reformulation of the EAM and SW potentials in a compatible functional form is discussed in this section. A reformulation of the conventional EAM potential into a form that includes three-body terms in the expression for the total electron density function is presented first, followed by the description of an approach for incorporation of the angular dependence compatible with the SW potential.

A. EAM potential with three-body terms in the electron density function

In the EAM potentials, the energy of an atom is expressed as

$$E_i = \frac{1}{2}\sum_{j\neq i} \phi_{ij}(r_{ij}) + F_i(\rho_i), \tag{1}$$

where r_{ij} is the distance between atoms i and j, $\phi_{ij}(r_{ij})$ is the pair energy term defined as a function of the interatomic distance, $F_i(\rho_i)$ is the embedding energy term defined as a function of the electron density ρ_i at the position of atom i, and the summation is over all atoms interacting with atom i. The electron density ρ_i is calculated as a sum of the partial electron density contributions from the neighboring atoms,

$$\rho_i = \sum_{j\neq i} f_j(r_{ij}), \tag{2}$$

where $f_j(r_{ij})$ is the partial electron density contribution from atom j at the location of atom i. Since only interatomic distances r_{ij} are needed to calculate the energy and forces in the system, the EAM calculations are nearly as simple and computationally efficient as the ones with pair potentials. The lack of explicit three-body terms, however, makes the conventional EAM inappropriate for covalently bonded materials.

To make the connections to SW or Tersoff potentials and to allow for the introduction of the angular dependence of the interatomic interactions, the linear sum of partial electron density contributions in Eq. (2) can be expressed through the sum of products of partial electron densities,

$$\rho_i = \left\{\left[\sum_{j\neq i} f_j(r_{ij})\right]^2\right\}^{1/2} = \left[\sum_{k\neq i}\sum_{j\neq i} f_j(r_{ij}) f_k(r_{ik})\right]^{1/2}. \tag{3}$$

The sum on the right-hand side of the above equation includes two-body terms with identical pairs of atoms ($j=k$) and three-body terms ($j\neq k$) that can be separated from each other.[28] The three-body terms can be written in the form of a sum over unique triplets of atoms (i,j,k),

$$\rho_i = \left\{\sum_{j\neq i} [f_j(r_{ij})]^2 + 2\sum_{j,k\subset T_i} f_j(r_{ij}) f_k(r_{ik})\right\}^{1/2}, \tag{4}$$

where in the first (two-body) term under the square root the summation is over all atoms interacting with atom i and in the second (three-body) term the summation is over all pairs of atoms j and k that form unique triplets with atom i. This formulation includes an explicit dependence on triplets of

neighboring atoms and, as shown in Sec. II B, allows for incorporation of the angular dependence of the interatomic interactions in a form compatible with Stillinger-Weber potential. Alternatively, the three-body terms can be written in a form of the "bond-order" dependence,

$$\rho_i = \left\{ \sum_{j\neq i} [f_j(r_{ij})]^2 + \sum_{j\neq i} f_j(r_{ij}) \sum_{k\neq i,j} f_k(r_{ik}) \right\}^{1/2}. \quad (5)$$

This formulation can be used to design an angular-dependent EAM potential compatible with the Tersoff potential.[29]

B. Angular-dependent EAM compatible with SW potential

The energy of an atom in a system described by SW potential is defined as[4]

$$E_i = \frac{1}{2}\sum_{j\neq i} U_2(r_{ij}) + \sum_{j,k\subset T_i} U_3(\vec{r}_i,\vec{r}_j,\vec{r}_k). \quad (6)$$

The potential consists of two-body (U_2) and three-body (U_3) terms, with the summation of the three-body terms being taken over all atom pairs j and k that form unique triplets with atom i. The two-body term has a Lennard-Jones form terminated at a distance r_c by a cutoff function

$$U_2(r_{ij}) = \varepsilon A \left[B\left(\frac{r_{ij}}{\sigma}\right)^{-p} - \left(\frac{r_{ij}}{\sigma}\right)^{-q} \right] \exp\left[\frac{\sigma}{r_{ij}-r_c}\right]. \quad (7)$$

The three-body term is defined as

$$U_3(\vec{r}_i,\vec{r}_j,\vec{r}_k) = \varepsilon\lambda \exp\left[\frac{\gamma\sigma}{r_{ij}-r_c} + \frac{\gamma\sigma}{r_{ik}-r_c}\right](\cos\theta_{jik} + 1/3)^2 \quad \text{for } r_{ij} < r_c,\ r_{ik} < r_c, \quad (8)$$

where θ_{jik} is an angle between vectors $\vec{r}_{ij}$ and $\vec{r}_{ik}$ originating from atom i and directed to atoms j and k. The parameters A, B, p, q, λ, ε, σ, γ, and r_c are adjustable parameters that are chosen to reproduce the properties of crystalline, liquid, and amorphous phases, as well as surface structures for Si or Ge.[4,5,30,31]

The sum of the three-body terms in Eq. (6) can be rewritten in a form of embedding energy,

$$F_i(\rho_i) = \sum_{j,k\subset T_i} U_3(\vec{r}_i,\vec{r}_j,\vec{r}_k) = \frac{\lambda\varepsilon}{2(f_e^{\mathrm{Si/Ge}})^2}\rho_i^2, \quad (9)$$

where the electron density and partial electron density contributions are defined as

$$\rho_i = \left[2\sum_{j,k\subset T} f_{ij}(r_{ij}) f_{ik}(r_{ik})(\cos\theta_{jik} + 1/3)^2 \right]^{1/2}, \quad (10)$$

$$f_{ij}(r_{ij}) = f_e^{\mathrm{Si/Ge}} \exp\left(\frac{\gamma\sigma}{r_{ij}-r_c}\right), \quad (11)$$

where $f_e^{\mathrm{Si/Ge}}$ is an adjustable parameter that cancels out in Eq. (9) for pure Si or Ge. Note that in the expression for the electron density given by Eq. (10), the partial electron density contributions are defined by the types of both atoms forming the bond, $f_{ij}(r_{ij})$, rather than the type of the neighboring atom, $f_j(r_{ij})$, as in the original EAM, Eq. (2). Moreover, the mutual contributions of two different atoms to the electron density at the locations of these atoms do not have to be the same, i.e., $f_{ij}(r_{ij}) \neq f_{ji}(r_{ij})$ for atoms i and j of different type. This assumption provides more flexibility in fitting the potential to the experimental data and the results of *ab initio* calculations, as discussed in Sec. III A, where an example of the parameterization procedure for cross interactions is given for Au-Si and Au-Ge systems.

Using the reformulation of the three-body terms of the SW potential in the functional form of the EAM embedding function, Eq. (9), and taking the pair energy term of the EAM potential in the form of the two-body term of the SW potential, $\phi_{ij}(r_{ij}) = U_2(r_{ij})$, the SW potential can be written in the form of the EAM potential, Eq. (1). For an alloy system containing both metal and Si/Ge atoms, a combined potential that reduces to the conventional SW and EAM potentials for pure components can be then formulated as follows:

$$E_i = \frac{1}{2}\sum_{j\neq i} \phi_{ij}(r_{ij}) + F_i\left[\left\{ (1-\delta_i)\sum_{j\neq i} [f_{ij}(r_{ij})]^2 + 2\sum_{j,k\subset T_i} f_{ij}(r_{ij}) f_{ik}(r_{ik})(\cos\theta_{jik} + 1/3)^{c_i} \right\}^{1/2} \right]. \quad (12)$$

Two parameters, δ_i and c_i, are added to ensure that the combined potential given by Eq. (12) reduces to the conventional EAM potential for pure metals and to the original SW potential for pure Si or Ge. For metals, $\delta_i = c_i = 0$ excludes the angular dependence and includes the radial contributions to electron density, thus, yielding the original EAM potential. For Si/Ge, $\delta_i = 1$ and $c_i = 2$ transform the electron density function into the three-body function of the SW potential, Eq. (10), that retains the angular dependence. As will be discussed in the next sections, the parameterization of the A-EAM potential for Au-Si/Ge interactions does not require an angular dependence of the electron density function for metal atoms. As a result, the computational efficiency of the evaluation of the A-EAM potential can be improved by rewriting the total electron density function in a form that does not involve the summation over triplets of neighboring atoms around a metal atom:

$$E_i = \frac{1}{2}\sum_{j\neq i} \phi_{ij}(r_{ij}) + F_i\left[\left\{ (1-\delta_i)\sum_{j\neq i} f_{ij}(r_{ij}) + c_i \sum_{j,k\subset T_i} f_{ij}(r_{ij}) f_{ik}(r_{ik})(\cos\theta_{jik} + 1/3)^2 \right\}^{n_i} \right]. \quad (12a)$$

Similarly to Eq. (12), the parameters are set to $\delta_i = c_i = 0$ for metals (the triplet contribution to electron density is eliminated) and $\delta_i = 1$ and $c_i = 2$ for Si/Ge (the radial contribution to the electron density is eliminated). The additional parameter n_i is equal to 1 for metals and 1/2 for Si/Ge. While in this work we use the formulation of the A-EAM potential given by Eq. (12a), the alternative formulation of Eq. (12) is useful when an angular dependence needs to be included in the electron density of metal atoms in order to provide an adequate representation of the interatomic interactions in metal-Si/Ge clusters and alloys.

The functional form and parameters of the embedding energy functions, $F_i(\rho_i)$, as well as the pair energy and partial

electron density functions for the interactions between atoms of the same type are directly defined by the original EAM and SW potentials and do not need to be adjusted in the alloy potential. The fitting of the alloy potential, therefore, is limited to finding the optimum parameters for the pair energy term, $\phi_{ij}(r_{ij})$, and the partial electron density contributions, $f_{ij}(r_{ij})$, for cross interactions between atoms of different type.

The angular dependence of interatomic interactions is incorporated into the alloy potential given by Eqs. (12) and (12a) in a form that is compatible with SW potential. Thus, this potential is referred to as the SW formulation of the A-EAM potential, or A-EAM (SW). An alternative approach for incorporation of the angular dependence, compatible with the Tersoff potential, is discussed elsewhere.[29]

III. A-EAM (SW) POTENTIAL FOR Au-Si/Ge

To test the ability of the combined A-EAM (SW) potential to reproduce the properties of systems with mixed metallic-covalent bonding in this section we provide an example of parameterization of the potential for Au-Si and Au-Ge systems.

A. Potential functions for pure components

Within the framework of the combined A-EAM (SW) potential, the embedding energy functions, the partial electron density functions, and the pair energy functions for pure components (Au, Si, and Ge) are uniquely defined by the original EAM and SW potentials. For pure Au, an EAM potential in the form suggested in Ref. 13 is used in this work. The advantage of this potential is in the simplicity of the functional form and the availability of parameterizations for many metals, allowing for an easy implementation for a broad range of alloy systems. For pure Si, the original parameterization of SW potential[4] is used. Various structural and thermodynamic characteristics of Si predicted by this potential have been thoroughly investigated, e.g., Refs. 4, 28, and 30–33 and found to be satisfactory for a broad range of applications. For Ge, a parameterization suggested in Ref. 5 provides a good representation of crystalline and amorphous solid phases but predicts grossly overestimated melting temperature (MD simulation of liquid-crystal coexistence yields a value of 2940 K, compared to the experimental value[34] of 1210 K). An alternative set of parameters that included parameter λ scaled down to 19.5 was proposed in Ref. 30. Although this parameterization decreases the melting temperature down to about 1090 K, it also reduces the anisotropy of the diffusion of Ge adatoms on a (2×1) reconstructed Si(001) surface to unrealistically low levels. In this work, we set the value of λ at 21.0 (the same as in Si of Ref. 4), keeping the rest of the parameters the same as in Ref. 5. This parameterization results in a melting temperature of about 1500 K and makes the anisotropy in the diffusion barriers for Ge adatoms on a (2×1) Si(001) surface to be similar to that for Si adatoms.

The parameter $f_e^{\mathrm{Si/Ge}}$ in the partial electron density function for the Si-Si and Ge-Ge contributions is set to a value of 16.0, so that Si, Ge, and Au have comparable partial electron density contributions in a range of distances around the equilibrium bond lengths of SW Si (2.34 Å), SW Ge (2.45 Å), and EAM Au (2.88 Å). As discussed below, the value of this parameter does not affect the fitting of the cross interactions and can be chosen arbitrarily. The plots of the embedding energy functions, the partial electron density functions, and the pair energy functions defining the interactions between atoms of the same type are shown for Au, Si, and Ge by solid lines in Figs. 1–3. The embedding energy in the equilibrium zero-temperature crystalline state is zero for A-EAM (SW) Si and Ge, whereas for Au the equilibrium state corresponds to the minimum of the embedding function. The antibonding nature of the embedding energy term for Si and Ge is a reflection of the main purpose served by this term in the A-EAM (SW) potential—to reproduce the energy penalty for deviations from perfect tetrahedral angles in the diamond lattice. The functional form and parameters of the pair energy functions and the electron density functions for cross interactions between atoms of different type are determined in this work based on the results of DFT calculations performed for several representative Au-Si/Ge bulk structures (Sec. III C) and small clusters (Sec. III D). The potential functions and parameters for Au-Si and Au-Ge cross interactions are discussed below in Sec. III B.

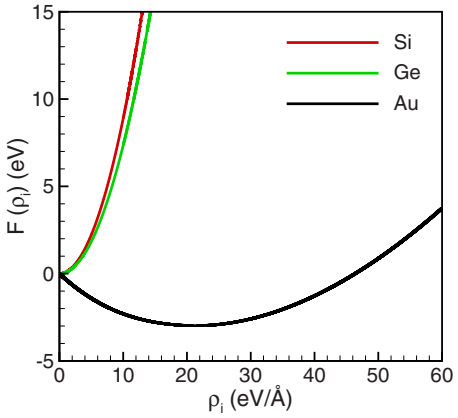

FIG. 1. (Color online) Plots of the embedding functions for EAM Au (black line), A-EAM (SW) Si (red line), and A-EAM (SW) Ge (green line).

B. Potential functions and parameters for Au-Si and Au-Ge cross interactions

The formulation of the A-EAM (SW) potential, given by Eq. (12a), implies that the presence of a Si/Ge atom contributes to the electron density of a neighboring metal atom only through the two-body term of the electron density function that does not have the angular dependence. On the other hand, the presence of a metal atom contributes to the electron density of a neighboring Si/Ge atom through the three-body (triplet interaction) term of the electron density function.

For Au-Si/Ge cross interactions, the pair energy term is defined in this work as

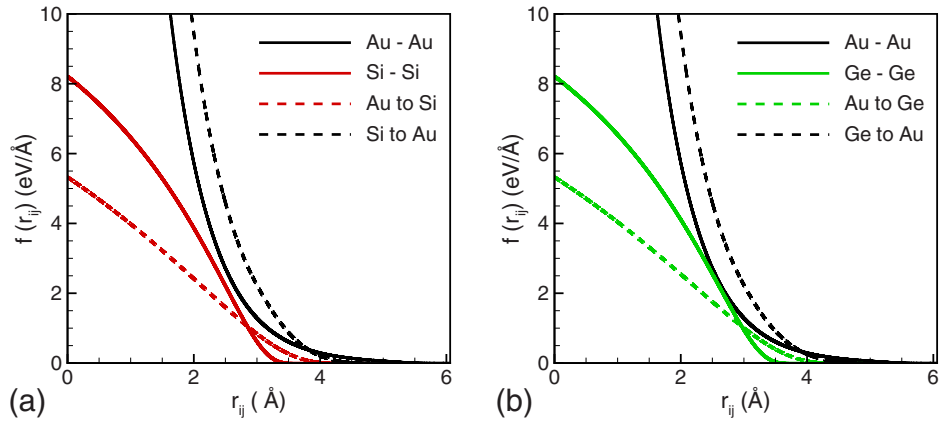

FIG. 2. (Color online) Plots of the partial electron density functions for (a) Si-Au and (b) Ge-Au interactions described by the A-EAM (SW) potential.

$$\phi_{ij}(r_{ij}) = A_C \exp\left[-\alpha_C\left(\frac{R_M}{r_{ij}-R_M}\right)\right]\left(\frac{r_{ij}}{\sigma_C}\right)^{-P_C} - B_C \exp\left[-\beta_C\left(\frac{R_M}{r_{ij}-R_M}\right)\right]\left(\frac{r_{ij}}{\sigma_C}\right)^{-Q_C}, \quad (13)$$

where A_C, B_C, α_C, β_C, σ_C, R_M, P_C, and Q_C are fitting parameters. The partial electron density contributions from a Au atom to a Si/Ge atom and from a Si/Ge atom to a Au atom are defined, respectively, as

$$f_{ij}^{\mathrm{Au}\to\mathrm{Si/Ge}}(r_{ij}) = f_e^{\mathrm{Si/Ge}} \exp\left\{-\gamma_C^{\mathrm{Si/Ge}}\left(\frac{R_M}{r_{ij}-R_M}\right)\right\} \quad (14)$$

and

$$f_{ij}^{\mathrm{Si/Ge}\to\mathrm{Au}}(r_{ij}) = f_e^{\mathrm{Au}}\left[\exp\left\{-\gamma_C^{\mathrm{Au}}\left(\frac{r_{ij}}{R_e^{\mathrm{Au}}}-1\right)\right\}\right] f_C(r_{ij}). \quad (15)$$

The function given by Eq. (14) is defined for the case when atom i is Si or Ge and atom j is Au, whereas the reverse is true for Eq. (15). The value of the parameter $f_e^{\mathrm{Si/Ge}}$ used in the calculation of the electron density contribution from Au to Si/Ge is chosen to be the same as the one used for the Si-Si and Ge-Ge contributions. This choice ensures that, based on Eqs. (10), (11), (12a), and (14), the parameter $f_e^{\mathrm{Si/Ge}}$ cancels out in the calculation of the embedding energy for Si/Ge atoms and can be assigned an arbitrary value. We keep this parameter in the potential as it may become useful when the potential is applied to different systems. The cutoff function, $f_C(r_{ij})$, is used in Eq. (15) to smoothly terminate the partial electron density contribution from Si to Au at $r_{ij} = R_M$. This function is taken in the form used in the Tersoff potential,[6,16]

$$f_C(r_{ij}) = \begin{cases} 1 & \text{for } 0 < r_{ij} < R_S \\ 1/2 + 1/2\cos\left[\pi\left(\dfrac{r_{ij}-R_S}{R_M-R_S}\right)\right] & \text{for } R_S < r_{ij} < R_M \\ 0 & \text{for } r_{ij} > R_M. \end{cases} \quad (16)$$

The fitting parameters in the partial electron density functions are f_e^{Au}, γ_C^{Au}, $\gamma_C^{\mathrm{Si/Ge}}$, R_e^{Au}, R_S, and R_M.

The parameters for the electron density function and the pair energy function for Au-Si and Au-Ge cross interactions, given by Eqs. (13)–(16), are selected based on the results of DFT calculations performed for several representative Au-

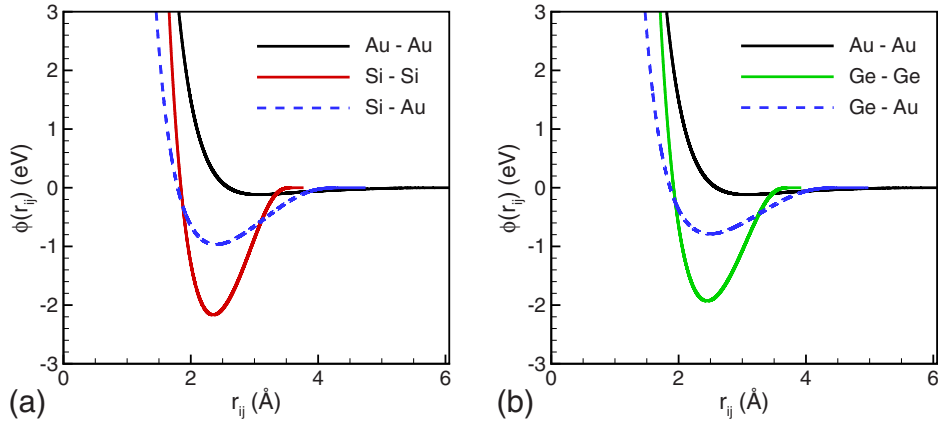

FIG. 3. (Color online) Plots of the pair potential functions for (a) Si-Au and (b) Ge-Au interactions described by the A-EAM (SW) potential.

TABLE I. Parameters of the pair energy function and the partial electron density function for Au-Si and Au-Ge cross interactions in the A-EAM (SW) potential.

Parameters	Au-Si	Au-Ge
A_C (eV)	5.189	4.769
B_C (eV)	9.8129	8.779
α_C	−0.555	−0.555
β_C	−0.93	−0.93
σ_C (Å)	1.81	1.884
P_C	4	4
Q_C	0	0
f_e^{Au}	4.8	4.2
$f_e^{\mathrm{Si/Ge}}$	16	16
γ_C^{Au}	3.56	3.56
$\gamma_C^{\mathrm{Si/Ge}}$	−1.1	−1.1
R_e^{Au} (Å)	2.47	2.57
R_S (Å)	2.97	3.07
R_M (Å)	4.7837	4.98

Si/Ge bulk structures and small clusters (see Secs. III C and III D). Since the number of the energy and structural parameters evaluated in the DFT calculations by far exceeds the number of the fitting parameters, the fitting procedure is not aimed at reproducing the exact values of the material properties predicted in the DFT calculations. Rather, the results of the DFT calculations and the experimental data on the enthalpy of mixing of liquid Au-Si and Au-Ge solutions[35] are considered together as a target in the optimization of the overall agreement. Two sets of parameters defining the cross-interaction functions in the A-EAM (SW) potential that are found to provide a satisfactory representation of the DFT results and the experimental enthalpies of mixing for Au-Si and Au-Ge systems (see Sec. IV) are listed in Table I. The corresponding plots of the partial electron density functions and the pair energy functions and are shown in Figs. 2 and 3 by the dashed lines.

As apparent from Fig. 2, the partial electron density contribution from Si to Au is larger than the ones from Au to Au and from Au to Si. Our initial attempt to use the same partial electron density contributions, $f_{ij}(r_{ij})=f_{ji}(r_{ij})$, resulted in unsatisfactory representation of some of the material properties, particularly the experimental dependence of the enthalpy of mixing of the liquid alloy on the composition. The large difference in the partial electron density contributions from Au to Si/Ge and from Si/Ge to Au can be loosely related to the partial charge transfer between the two components. The DFT calculations discussed in the following sections suggest that the formation of a Au-Si/Ge bond is associated with a partial charge transfer from the Si or Ge atom to the Au atom. This observation is consistent with the results of recent DFT calculations performed for a Au/Si interface,[36] which show that an extra charge density is supplied to Au-Si bonds by the neighboring Si-Si bonds. The charge transfer from Si/Ge to Au can be attributed to higher electronegativity of Au as compared to Si and Ge, 2.54 vs 1.90 and 2.01 in Pauling units.

The connection between the actual electron density in the atomic configurations and the concept of the "electron density" used in the formulation of the EAM potential, however, is rather tortuous and may be misleading. It is more important to consider how the difference in the partial electron density contributions affects the performance of the A-EAM (SW) potential. According to Eq. (12a), the reduction in the electron density at the location of a Si/Ge atom due to the presence of Au atoms in its neighborhood corresponds to the weakening of the strength of the angular interactions, increasing the tolerance of the local configuration to deviations from the perfect diamond lattice structure. On the other hand, the higher values of the electron density contribution from Si/Ge to Au, as compared to Au to Au contribution, imply that a Au atom has an increased electron density and, therefore, more repulsive interactions with the neighboring atoms, when it has Si/Ge atoms as its neighbors. A quantitative analysis of the performance of the A-EAM (SW) potential with cross interaction defined by the parameters given in Table I is provided in the following sections, where the predictions of the A-EAM (SW) potential are related to the results of DFT calculations and experimental data.

C. DFT calculations for bulk Au, Si, Ge, and their alloys

Plane-wave periodic density-functional theory calculations, as implemented in the Vienna *ab initio* simulation package (VASP) code,[37] are used to calculate structural and energy characteristics of various bulk crystals and model Au-Si and Au-Ge alloys. The calculations are carried out using the Perdew-Wang 1991 (PW91) functional[38] within generalized gradient approximation (GGA) and the local-density approximation (LDA). The interactions between ions and electrons are described by the ultrasoft Vanderbilt pseudopotentials[39] provided in the VASP program.[37] The cutoff energy used for the plane-wave basis set is 200.0 eV. The electronic energy is converged to within a tolerance of 10^{-4} eV, whereas the structures are optimized to within 10^{-3} eV.

The total bonding energies for the alloys (Au-Si or Au-Ge) were calculated by subtracting the sum of the energies of individual atoms (E_{Si}, E_{Ge}, and E_{Au}) from the calculated energy of the specific alloy considered (E_{alloy}). For example, for a Au-Si alloy configuration consisting of N_{Si} silicon atoms and N_{Au} gold atoms, the total energy (E_{Tot}) is defined as

$$E_{Tot} = E_{alloy} - (N_{\mathrm{Si}}E_{\mathrm{Si}} + N_{\mathrm{Au}}E_{\mathrm{Au}}). \tag{17}$$

The cohesive energy of the alloy is defined as the average bonding energy per atom, $E_C=E_{Tot}/(N_{\mathrm{Si}}+N_{\mathrm{Au}})$. The calculation of the energies of individual atoms (E_{Si} and E_{Au}) includes spin-polarization effects. The bulk modulus (B) is determined by calculating the total energy as a function of volume (V) and fitting the total energy versus volume dependence, $E_{Tot}(V)$, to the Birch-Murnaghan equation of state.[40,41]

The calculations for the alloy systems are preceded by evaluation of the performance of the GGA and LDA calculations in predicting properties of one-component systems. The lattice constant (a_o), cohesive energy, and bulk modulus

TABLE II. The values of the lattice constant, a_o, the cohesive energy, E_C, and the bulk modulus, B, predicted for Si, Ge, and Au crystals (diamond lattice for Si and Ge, fcc for Au) in DFT (VASP) calculations performed with GGA (PW91) and LDA. The results of the DFT calculations are compared with predictions of the A-EAM (SW) potential, as well as with experimental values (Ref. 34).

Elements/Property		GGA	LDA	A-EAM (SW)	Experiment[a]
Si	a_o (Å)	5.445	5.393	5.431	5.431
	E_C (eV/atom)	−4.560	−5.285	−4.334	−4.630
	B (Mbar)	0.851	0.957	1.014	0.980
Ge	a_o (Å)	5.764	5.629	5.65	5.650
	E_C (eV/atom)	−3.745	−4.563	−3.860	−3.860
	B (Mbar)	0.584	0.712	0.795	0.772
Au	a_o (Å)	4.183	4.068	4.089	4.089
	E_C (eV/atom)	−3.106	−4.186	−3.930	−3.930
	B (Mbar)	1.301	1.850	1.664	1.670

[a]Reference 34.

are calculated for Si, Ge, and Au crystals with diamond cubic structure for Si and Ge and face-centered cubic (fcc) structure for Au. The results are summarized and compared with experimental data,[34] as well as with values predicted by the A-EAM (SW) potential, in Table II. The values obtained for Si agree with the results of DFT calculations reported in Ref. 42. The comparison of the results of the DFT calculations with experimental data suggests that GGA provides a better description of the cohesive energies of Si and Ge, whereas LDA is more accurate in predicting the lattice constants and bulk moduli of Ge and Au, as well as the cohesive energy of Au. Therefore, in order to achieve an overall good representation of the structural characteristics and energies of bulk alloys, a combination of the results of GGA and LDA calculations is used in the parameterization of Au-Si and Au-Ge cross interactions in the A-EAM (SW) potential.

In the absence of stable Au-Si and Au-Ge alloy compounds, the results of DFT calculations performed for two artificial cubic crystal structures, B1 (AuSi, AuGe) and $L1_2$ (Au_3Si, Au_3Ge), are used in the parameterization of the potential. The values of lattice constants, cohesive energies, and bulk moduli predicted in LDA and GGA calculations for the two structures are listed for the Au-Si and Au-Ge systems in Tables III and IV, respectively. The energy difference between a substitutional Au impurity and a vacancy in Si and Ge diamond lattices ($E_{vac}^{Sub/Au}$) is also calculated and listed in the tables.

The results of the calculations performed for the same atomic structures with A-EAM (SW) potential are also given in Tables III and IV. The empirical potential with the sets of parameters listed in Table I is found to provide an overall satisfactory description of the DFT results. The values predicted for the lattice constants and the energy differences between substitutional Au impurities and vacancies in the Si and Ge crystals are slightly larger than the values predicted in the DFT calculations, whereas the cohesive energies and bulk moduli tend to fall in between the values predicted in the GGA and LDA calculations.

D. DFT calculations for small Au-Si and Au-Ge clusters

In addition to the bulk systems discussed in the previous section, the results of DFT calculations for small (five-atom) clusters ($AuSi_4, AuGe_4$) are used in parameterization of the A-EAM (SW) potential. The calculations are performed for three cluster configurations shown in Fig. 4, namely, tetrahedral (Tetra), pentagonal (Penta), and close packed (CP). The geometry of the clusters is characterized by one (a_0 in Tetra) or two (a_1 and a_2 in Penta and CP) Au-Si/Au-Ge interatomic distances, as well as Si-Au-Si/Ge-Au-Ge bond angles

TABLE III. Properties of two artificial crystal structures, B1 (AuSi) and $L1_2$ (Au_3Si) predicted in DFT (VASP) calculations performed with GGA and LDA, as well as in simulations performed with the A-EAM (SW) potential. The values of the lattice constant, a_o, the cohesive energy, E_C, the bulk modulus, B, and the energy difference between a substitutional Au impurity and a vacancy in Si diamond lattice, $E_{vac}^{Sub/Au}$, are listed in the table.

		$L1_2$			B1		
Au-Si	$E_{vac}^{Sub/Au}$ (eV)	a_o (Å)	E_C (eV/atom)	B (Mbar)	a_o (Å)	E_C (eV/atom)	B (Mbar)
GGA	5.919	4.145	−3.149	1.203	5.280	−3.643	0.845
LDA	6.944	4.087	−4.108	1.888	5.198	−4.250	0.925
A-EAM (SW)	7.024	4.193	−4.035	1.591	5.362	−3.873	1.018

TABLE IV. Properties of two artificial crystal structures, B1 (AuGe) and $L1_2$ (Au_3Ge) predicted in DFT (VASP) calculations performed with GGA and LDA, as well as in simulations performed with the A-EAM (SW) potential. The values of the lattice constant, a_o, the cohesive energy, E_C, the bulk modulus, B, and the energy difference between a substitutional Au impurity and a vacancy in Ge diamond lattice, $E_{vac}^{Sub/Au}$, are listed in the table.

		$L1_2$			B1		
Au-Ge	$E_{vac}^{Sub/Au}$ (eV)	a_o (Å)	E_C (eV/atom)	B (Mbar)	a_o (Å)	E_C (eV/atom)	B (Mbar)
GGA	5.470	4.212	−3.179	1.019	4.455	−3.354	0.791
LDA	6.190	4.090	−4.185	1.437	5.302	−4.302	0.896
A-EAM (SW)	6.56	4.259	−3.860	1.275	5.472	−3.660	0.870

$(\theta_{\text{Si-Au-Si}}, \theta_{\text{Ge-Au-Ge}})$ calculated for the Penta configuration.

All DFT calculations (GGA and LDA) for small clusters are performed with DMol³ module of the Accelrys MATERIALS STUDIO software package. A double numerical basis set is used to describe all atoms, which includes polarization functions along with effective core potentials to model the core electrons. All of the GGA calculations are performed using the PW91 functional. Relativistic effects are treated using relativistic core pseudopotentials. The structures of individual clusters are optimized with a self-consistent field energy convergence of 1.0×10^{-7} hartree. The total energies, interatomic distances, and bond angles are found by optimizing the structures to within a 10^{-7} hartree tolerance using DMol³. Similarly to the energies of bulk structures, Eq. (17), the total energy, E_T, of a cluster consisting of $N_{\text{Si/Ge}}$ Si or Ge atoms and N_{Au} Au atoms is obtained by subtracting the sum of the energies of the individual atoms (E_{Si}, E_{Ge}, and E_{Au}) from the total energy of the cluster predicted by DMol³ ($E_{cluster}$),

$$E_T = E_{cluster} - (N_{\text{Si/Ge}}E_{\text{Si/Ge}} + N_{\text{Au}}E_{\text{Au}}). \quad (18)$$

The results of the DFT calculations and the corresponding predictions of the A-EAM (SW) potential are summarized in Tables V and VI for $AuSi_4$ and $AuGe_4$ clusters, respectively. Out of the three configurations considered for $AuSi_4$ and $AuGe_4$ clusters, the close-packed configuration is predicted to have the lowest energy in both GGA and LDA calculations. This prediction is in agreement with the results obtained with the A-EAM (SW) potential. The equilibrium bond angles, predicted by the A-EAM (SW) potential for the pentagonal configuration, however, exhibit significant deviation from the values obtained in the GGA and LDA calculations. Nevertheless, given the uncertainty in the quantitative accuracy of the DFT calculations, the overall performance of the empirical potential in the description of the crystal structures and small clusters can be considered to be acceptable. An important test of the suggested parameterization of the A-EAM (SW) potential comes from the calculation of the properties of liquid Au-Si and Au-Ge alloys, for which experimental data are available.[35] The results of the calculations of the enthalpies of mixing of liquid Au-Si and Au-Ge alloys and the equilibrium lines on the Au-Si phase diagram are presented and compared with experimental data in the next two sections.

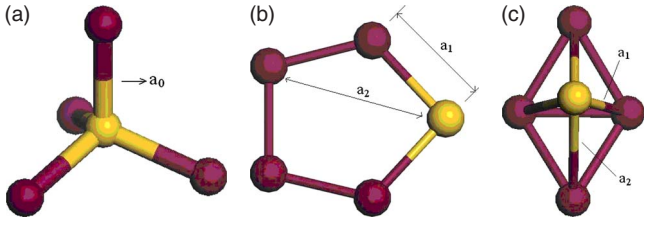

FIG. 4. (Color online) (a) Tetrahedral, (b) pentagonal, and (c) close-packed configurations of $AuSi_4$ and $AuGe_4$ clusters analyzed in DFT (DMol³) and A-EAM (SW) calculations. Interatomic distances that characterize the geometry of the clusters are shown in the figures. The Au and Si/Ge atoms are shown in yellow and maroon colors, respectively.

IV. ENTHALPY OF MIXING OF LIQUID Au-Si AND Au-Ge ALLOYS

The dependence of the enthalpy of mixing on the composition of the alloys is calculated for a temperature of 1500 K for Au-Si and for a temperature of 1685 K for Au-Ge. The corresponding sets of experimental data are available for these alloys in Ref. 35, allowing for the direct comparison between the calculated and experimental dependences. The

TABLE V. Structural characteristics and energies of three $AuSi_4$ clusters shown in Fig. 4, as predicted in DFT (DMol³) calculations performed with GGA and LDA, as well as in simulations performed with A-EAM (SW) potential. Here, a_o, a_1, and a_2 are the Au-Si interatomic distances marked in Fig. 4, E_T is the total energy of the cluster, and $\theta_{\text{Si-Au-Si}}$ is the Si-Au-Si bond angle in the pentagonal configuration.

$AuSi_4$ cluster		GGA	LDA	A-EAM (SW)
Tetra	a_0 (Å)	2.398	2.356	2.396
	E_T (eV)	−7.7092	−10.044	−6.84733
Penta	a_1/a_2 (Å)	2.32/3.94	2.278/3.842	2.220/3.544
	E_T (eV)	−13.353	−15.535	−11.188
	$\theta_{\text{Si-Au-Si}}$ (deg)	94.403	94.968	120.309
CP	a_1/a_2 (Å)	2.754/2.983	2.677/2.866	2.521/3.035
	E_T (eV)	−13.686	−15.791	−11.5817

TABLE VI. Structural characteristics and energies of three $AuGe_4$ clusters shown in Fig. 4, as predicted in DFT (DMol[3]) calculations performed with GGA and LDA, as well as in simulations performed with A-EAM (SW) potential. Here, a_o, a_1, and a_2 are the Au-Ge interatomic distances marked in Fig. 4, E_T is the total energy of the cluster, and $\theta_{\text{Ge-Au-Ge}}$ is the Ge-Au-Ge bond angle in the pentagonal configuration.

$AuGe_4$ cluster		GGA	LDA	A-EAM (SW)
Tetra	a_o (Å)	2.482	2.429	2.451
	E_T (eV)	−7.259	−9.6514	−6.3623
Penta	a_1/a_2 (Å)	2.722/4.790	2.584/4.658	2.533/4.158
	E_T (eV)	−10.521	−12.935	−10.105
	$\theta_{\text{Ge-Au-Ge}}$ (deg)	68.569	66.502	102.502
CP	a_1/a_2 (Å)	2.837/3.102	2.743/2.984	2.656/3.284
	E_T (eV)	−12.377	−14.7046	−10.430

values of the enthalpy of mixing are obtained in MD simulations performed for a system composed of 500 atoms initially arranged in an fcc lattice with dimensions of $5\times5\times5$ unit cells. The relative fractions of Au and Si/Ge atoms in the atomic configuration defined the composition of the system. For each composition, the liquid structure is prepared by slow heating performed up to the temperature when a complete meting of the system is observed. The simulations are performed under zero pressure conditions, allowing the system to change volume during heating and melting. The liquid structure is then equilibrated for 200 ps at a temperature of interest. The enthalpy of mixing at zero pressure is calculated from the internal energy of the liquid alloy. For example, the molar enthalpy of mixing of the Au-Si alloy at temperature T and molar fraction of silicon X_{Si} is calculated as

$$\Delta H_{mix}(X_{\text{Si}},T) = U(X_{\text{Si}},T) - [X_{\text{Si}}U_{\text{Si}}(T) + (1-X_{\text{Si}})U_{\text{Au}}(T)], \tag{19}$$

where $U_{\text{Si}}(T)$ and $U_{\text{Au}}(T)$ are the molar internal energies of pure liquid Si and pure liquid Au, respectively, and $U(X_{\text{Si}},T)$ is the molar internal energy of the alloy.

The calculated and experimental dependences of the enthalpy of mixing of Au-Si and Au-Ge liquid alloys on the composition of the alloys are shown in Fig. 5. The dependences obtained with the A-EAM (SW) potential capture the main characteristics of the experimental dependences. In particular, in agreement with experimental dependences, the calculated curves have asymmetric shapes, with minima shifted to the Au-rich side of the alloy compositions. The dependence calculated for Au-Si has a minimum of −9.88 kJ/mol at a concentration of 33 at. % Si and is in a good semiquantitative agreement with the experimental dependence exhibiting a minimum of −8.23 kJ/mol at a composition of 24 at. % Si. The agreement is even better for Au-Ge alloy, where the calculated dependence has a minimum of −6.68 kJ/mol at a concentration of 39 at. % Si, compared to the experimental dependence exhibiting a minimum of −5.4 kJ/mol at a composition of 38 at. % Ge. To further test the ability of the A-EAM (SW) potential to describe the thermodynamic properties of metal-covalent systems, the results of the calculation of the equilibrium phase diagram for the Au-Si alloy are discussed in the next section.

V. PHASE DIAGRAM OF Au-Si ALLOY

The domains of thermodynamic stability of phases can be established for the Au-Si system by calculating the Gibbs free energy - composition (G-X) curves for all phases present in the system at various temperatures.[43] The equilibrium lines on the phase diagram can then be obtained using the common tangent construction applied to sets of G-X curves plotted for different phases at the same values of temperature.

The Gibbs free energy of mixing of a binary Au-Si alloy under constant pressure conditions can be written as

$$\Delta G_{mix}(X_{\text{Si}},T) = \Delta G^{ex}_{mix}(X_{\text{Si}},T) + k_B T[X_{\text{Si}}\ln(X_{\text{Si}}) + (1-X_{\text{Si}})\ln(1-X_{\text{Si}})], \tag{20}$$

where k_B is the Boltzmann constant and ΔG^{ex}_{mix} is the excess free energy of mixing.[43] Within the regular solution model, the excess free energy of mixing can be approximated by the enthalpy of mixing, which can be easily evaluated in MD

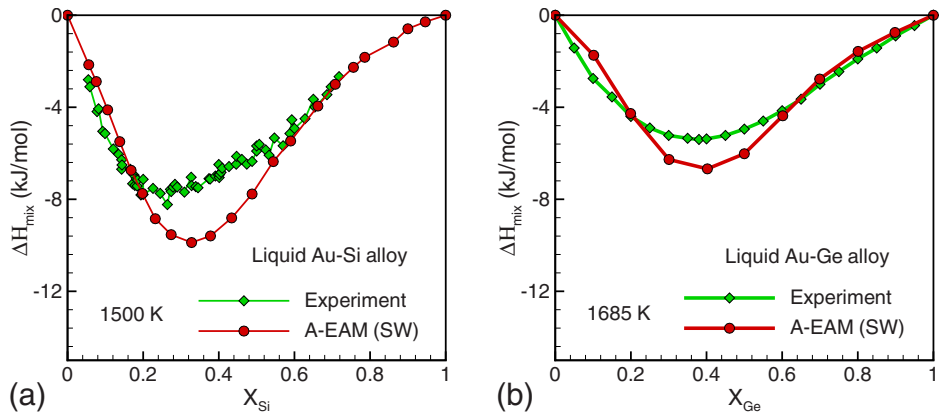

FIG. 5. (Color online) Enthalpy of mixing of (a) liquid Au-Si alloy at 1500 K and (b) liquid Au-Ge alloy at 1685 K. The values predicted by the A-EAM (SW) potential are shown by red circles and experimental data (Ref. 35) is shown by green diamonds.

simulations performed for different temperatures and compositions (see Sec. IV). The large difference in atomic sizes of Au and Si, along with other contributions to the excess entropy,[44,45] however, may result in the entropy of mixing significantly exceeding that of an ideal solution, making the above approximation unreliable.[46] Therefore, the excess Gibbs free energy of mixing is calculated in this work based on the results of semi-grand canonical MC (SGCMC) simulations,[47–50] as discussed below.

The SGCMC simulations provide a convenient method for evaluation of the difference in the excess chemical potentials of Au and Si, $\Delta\mu_{ex}=\mu^{ex}_{\mathrm{Au}}-\mu^{ex}_{\mathrm{Si}}$. To calculate the excess chemical potential difference for a given phase state, the initial systems are first prepared and equilibrated in MD simulations performed at zero pressure and desired temperatures and compositions. In the subsequent MD simulation, we perform a series of virtual trial MC moves, where each move corresponds to a virtual switch in the identity of a randomly selected Si atom to Au. The change in the potential energy of the system $\Delta U_{\mathrm{Si}\rightarrow\mathrm{Au}}$ and the corresponding Boltzmann factor $\exp(-\Delta U_{\mathrm{Si}\rightarrow\mathrm{Au}}/k_BT)$ associated with the switch are calculated and the identity of the atom is switched back to Si. In this combined MD-MC approach, the constant-pressure constant-temperature MD serves the purpose of providing equilibrium configurations for the execution of the virtual switches of the SGCMC algorithm. A commonly used alternative for exploring the configurational space is to include random displacements of atoms and random changes in volume of the computational cell in the MC simulation.[47,48,50] We verified the equivalence of the two approaches by performing MD-MC calculations of the boundary outlining the solid phase-separation regions (miscibility gaps) in the low-temperature parts of the phase diagrams for SW and Tersoff Si-Ge and comparing the results to the predictions of earlier SGCMC calculations.[15,51]

After a large number of the virtual trail moves is performed, the excess chemical potential difference can be calculated using the following equation,[47]

$$\Delta\mu_{ex}=-k_BT\ln\left\langle\frac{N_{\mathrm{Si}}}{N_{\mathrm{Au}}+1}\exp\left(-\frac{\Delta U_{\mathrm{Si}\rightarrow\mathrm{Au}}}{k_BT}\right)\right\rangle, \quad (21)$$

where N_{Au} and N_{Si} are the number of Au and Si atoms in the system. Once $\Delta\mu_{ex}$ is calculated for different temperatures and compositions of the alloy, the excess Gibbs free energy of mixing can be obtained from the Gibbs-Duhem equation, by integrating the excess chemical potential difference

$$\frac{\partial}{\partial X_{\mathrm{Si}}}[\Delta G^{ex}_{mix}(X_{\mathrm{Si}},T)]=-\Delta\mu_{ex}(X_{\mathrm{Si}},T). \quad (22)$$

For the Au-Si system, the three phases that have to be considered are the α (fcc) phase, the β (diamond cubic) phase, and the L (liquid) phase. The Gibbs free energies of mixing obtained for these three phases from Eqs. (20)–(22) have different reference states (phases of the pure components before mixing). Using notation that explicitly shows the reference states for the two components in the brackets,[43] the Gibbs free energies of mixing for the three phases are $\Delta G^{\alpha}_{mix}\{\alpha;\alpha\}$, $\Delta G^{\beta}_{mix}\{\beta;\beta\}$, and $\Delta G^{L}_{mix}\{L;L\}$. To enable a direct comparison of the Gibbs free energies of mixing of these three phases, the same reference state should be used for each of the two components in all three cases. Choosing the reference states as pure fcc α for Au, and pure diamond cubic β for Si, the Gibbs free energies of mixing can be written as

$$\Delta G^{\alpha}_{mix}\{\alpha;\beta\}=\Delta G^{\alpha}_{mix}\{\alpha;\alpha\}+X_{\mathrm{Si}}\Delta G^{0\beta\rightarrow\alpha}_{\mathrm{Si}}, \quad (23)$$

$$\Delta G^{\beta}_{mix}\{\alpha;\beta\}=\Delta G^{\beta}_{mix}\{\beta;\beta\}+(1-X_{\mathrm{Si}})\Delta G^{0\alpha\rightarrow\beta}_{\mathrm{Au}}, \quad (24)$$

$$\Delta G^{L}_{mix}\{\alpha;\beta\}=\Delta G^{L}_{mix}\{L;L\}+(1-X_{\mathrm{Si}})\Delta G^{0\alpha\rightarrow L}_{\mathrm{Au}}+X_{\mathrm{Si}}\Delta G^{0\beta\rightarrow L}_{\mathrm{Si}}, \quad (25)$$

where $\Delta G^{0\beta\rightarrow\alpha}_{\mathrm{Si}}=G^{0\alpha}_{\mathrm{Si}}-G^{0\beta}_{\mathrm{Si}}$, $\Delta G^{0\alpha\rightarrow\beta}_{\mathrm{Au}}=G^{0\beta}_{\mathrm{Au}}-G^{0\alpha}_{\mathrm{Au}}$, $\Delta G^{0\alpha\rightarrow L}_{\mathrm{Au}}=G^{0L}_{\mathrm{Au}}-G^{0\alpha}_{\mathrm{Au}}$, and $\Delta G^{0\beta\rightarrow L}_{\mathrm{Si}}=G^{0L}_{\mathrm{Si}}-G^{0\beta}_{\mathrm{Si}}$ are the differences in the Gibbs free energies of different phases for the corresponding pure components.

The application of the combined MD-MC approach for calculation of the Gibbs free energies of mixing for the solid phases, Eqs. (23) and (24), is hampered by the loss of stability of the solid phases with solute concentrations exceeding 20 at. % in MD simulations performed at 300 K or above. The high energy of Si substitutional impurities in fcc Au and Au substitutional impurities in diamond cubic Si, along with the limited stability of the solid solutions at finite temperatures, suggest that the Gibbs free energies of mixing given by Eqs. (23) and (24) are increasing sharply and become positive at small concentrations of solute atoms, thus allowing to assume that Au and Si are mutually insoluble in the solid state at all temperatures. This assumption eliminates the need for calculations of the G-X curves for the solid phases, as the common tangent construction can be drawn to the end points of the range of composition ($X_{\mathrm{Si}}=0$ and $X_{\mathrm{Si}}=1$). The lack of mutual solubility of Au and Si in the solid state is also observed experimentally,[35] with less than 2 at. % Si soluble in Au and less than 2×10^{-4} at. % Au in Si.

The Gibbs free energy of mixing in the liquid state, $\Delta G^{L}_{mix}\{L;L\}$, is calculated based on the results of SGCMC simulations, Eqs. (20)–(22), as discussed above. To illustrate the calculation procedure, the values of the excess chemical potential difference, $\Delta\mu_{ex}$, obtained in the SGCMC simulations for the liquid alloy at 700 and 1100 K are shown in Figs. 6(a) and 6(b), respectively. The excess Gibbs free energy of mixing, $\Delta G^{ex}_{mix}(X_{\mathrm{Si}},T)$, is then calculated with Eq. (22) and used in Eq. (20) to obtain the Gibbs free energy of mixing of the liquid alloy. The final step is to change the reference states in the expression of the Gibbs free energy of mixing from the liquid phase components to the α phase for Au and β phase for Si, Eq. (25). This change in the reference states requires knowledge of the corresponding differences in the Gibbs free energies of pure components in the solid and liquid states. The values of $\Delta G^{0\alpha\rightarrow L}_{\mathrm{Au}}$ and $\Delta G^{0\beta\rightarrow L}_{\mathrm{Si}}$ are calculated in this work based on the results of MD simulations performed for fcc Au, diamond cubic Si, and liquid phase Au and Si. The simulations are performed under constant pressure conditions for ranges of temperatures limited by the temperatures of maximum superheating for the solid phases and by the temperatures of the maximum undercooling be-

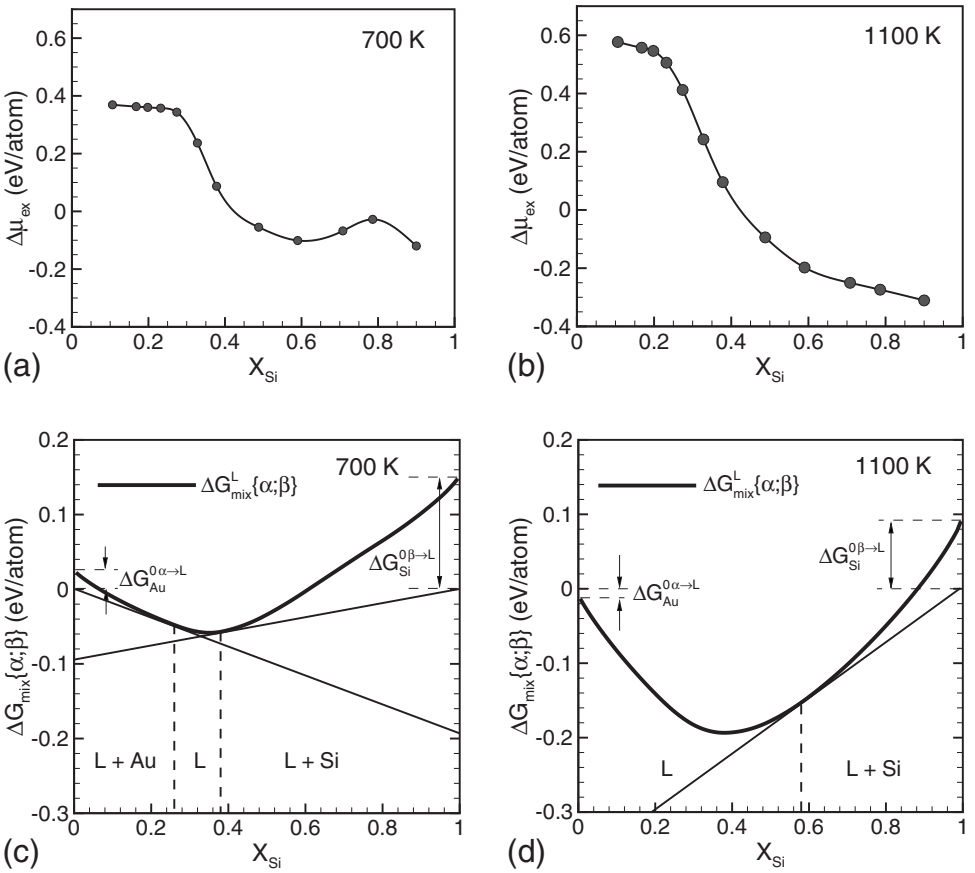

FIG. 6. Plots of the excess chemical potential difference and the Gibbs free energy of mixing calculated for the liquid Au-Si alloy based on the results of SGCMC simulations. Interatomic interactions are described by the A-EAM (SW) potential. The results are presented for two temperatures, [(a) and (c)] 700 K and [(b) and (d)] 1100 K. The tangent lines drawn in (c) and (d) to the *G-X* curve for the liquid phase define the boundaries of liquid-solid coexistence regions (liquidus lines shown in Fig. 7).

fore the onset of crystallization for the liquid phases. Using a procedure described in Ref. 52, the temperature dependences of the heat capacity are calculated for the liquid and solid phases from the temperature dependences of the enthalpy obtained in MD simulations, $C_P=(\partial H/\partial T)_P$. The temperature dependences of the heat capacity are then used to calculate the temperature dependences of the entropy for the four phases. The reference values for the enthalpy and entropy temperature dependences for the liquid phases are obtained from the values of the latent heat of melting, ΔH_m, and the entropy change in melting, $\Delta S_m=\Delta H_m/T_m$, with the equilibrium melting temperatures, T_m, determined in a separate set of liquid-crystal coexistence simulations performed for EAM Au and SW Si. The Gibbs free energies of pure components are then determined from the values of the enthalpy and entropy, and the changes in the Gibbs free energy upon melting of Au and Si are obtained for different temperatures as $\Delta G=\Delta H-T\Delta S$.

Once all the terms of Eq. (25) are known, the *G-X* curves for the liquid phase can be plotted for different temperatures and the common tangent constructions can be used to determine the equilibrium lines on the phase diagram. The plots of the *G-X* curves and the common tangent constructions are shown for temperatures of 700 and 1100 K in Figs. 6(c) and 6(d), respectively. The temperature of 700 K is below the melting temperatures of both EAM Au (963 K) (Ref. 52) and SW silicon (1677 K).[53] As a result, the liquid curve has positive end points at both $X_{Si}=0$ ($\Delta G^{0\alpha\to L}_{Au}>0$) and $X_{Si}=1$ ($\Delta G^{0\beta\to L}_{Si}>0$). As discussed above, due to the lack of mutual solubility of Au and Si in the solid state, the *G-X* curves for the solid phases are assumed to have their minima very close to the compositions of pure components. The common tangent constructions are then reduced to tangent lines drawn from the points corresponding to pure α and β phases ($\Delta G^{\alpha}_{mix}\{\alpha;\beta\}=0$, $X_{Si}=0$ and $\Delta G^{\beta}_{mix}\{\alpha;\beta\}=0$, $X_{Si}=1$) to the curves corresponding to the liquid phase ($\Delta G^{L}_{mix}\{\alpha;\beta\}$). Each common tangent construction gives a point on a liquidus line below which the liquid solution is in equilibrium with the corresponding solid phase. The temperature of 1100 K is above the melting temperature of Au but below the melting temperature of Si. Thus, only one common tangent construction can be drawn in Fig. 6(d), defining the boundary of the liquid-solid Si coexistence region on the phase diagram.

The equilibrium phase diagram predicted by the A-EAM (SW) potential for the Au-Si system is shown in Fig. 7(a). The liquidus lines on the phase diagram are obtained by computing the Gibbs free energy of mixing for the liquid phase at different temperatures, and then using the common tangent construction, as described above. The phase diagram is of the simple eutectic type and matches relatively well the

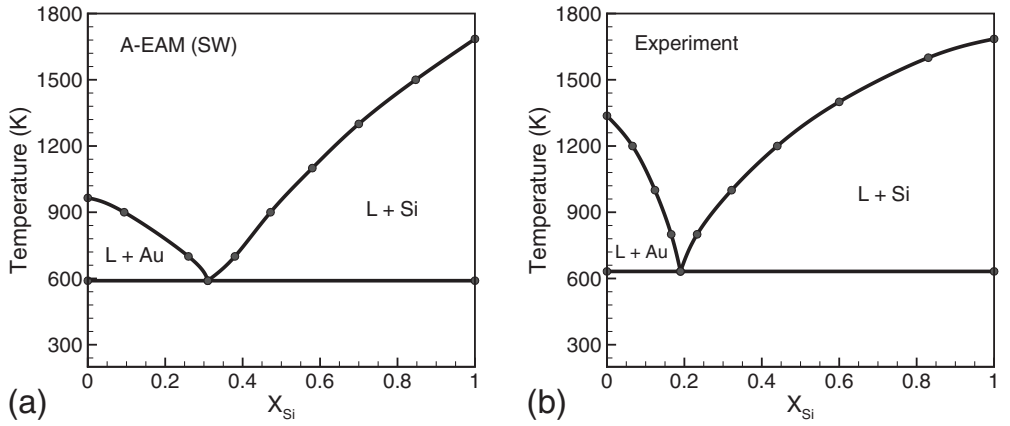

FIG. 7. Phase diagrams of the Au-Si alloy as (a) predicted by the A-EAM (SW) potential and (b) obtained experimentally (Ref. 35). The eutectic temperatures and compositions are 590 K and 31 at. % Si in (a) and 636 K and 18.6 at. % Si in (b).

experimental phase diagram shown in Fig. 7(b). The A-EAM (SW) potential predicts a eutectic temperature of 590 K, which is comparable to the experimental eutectic temperature of 636 K. The eutectic composition of 31 at. % Si, predicted by the A-EAM (SW) potential, however, exhibits a substantial deviation from the experimental value of 18.6 at. % Si. The overestimation of the eutectic composition and underestimation of the eutectic temperature can be attributed to the lower melting point of the EAM Au material (963 K determined in MD simulations,[52] as compared to the experimental value[34] of 1338 K), as well as to the shift of the location of the minimum of the composition dependence of the enthalpy of mixing to higher values of Si concentration compared to the experimental data, Fig. 5(a). Thus, a more accurate fitting of the Au-Si cross interaction to the enthalpy of mixing of the liquid alloy, along with improved melting properties of the EAM Au can be expected to result in a more accurate representation of the experimental Au-Si phase diagram by the A-EAM (SW) potential.

VI. SUMMARY

A relatively simple and computationally efficient description of interatomic interactions in metal-covalent systems can be achieved with an angular-dependent embedded atom method potential combining the EAM potential with the SW potential in a compatible form. The design of the A-EAM (SW) potential involves a reformulation of the electron density function of the conventional EAM potential to include an explicit three-body angular dependence. The effects related to the charge transfer in the interactions between atoms with different electronegativities can be accounted for in the potential by defining the partial electron density contributions based on the type of the pair of atoms forming a bond, rather than the types of individual atoms.

The A-EAM (SW) potential reduces to well-established and thoroughly tested potentials developed for pure components and provides an attractive alternative to the design of new alloy potentials with original functional forms. The functional form and parameters used in the description of the interactions between atoms of the same type are directly defined by the original EAM and SW potentials and do not need to be adjusted in the alloy potential, thus eliminating the need for extensive testing and limiting the scope of the potential parameterization to only the cross interaction between the components. Moreover, the A-EAM (SW) potential allows for an easy extension to multicomponent systems for which the EAM and SW potentials have been parameterized. For example, the EAM potential used in this work for Au has also been parameterized for 15 other metals[13] with simple alloy model enabling simulations of multicomponent metallic alloys. With the development of the A-EAM (SW) potential, the range of alloy systems accessible for atomistic modeling can be expanded to include Si and Ge.

The ability of the potential to provide an adequate description of binary systems with mixed metallic-covalent type of bonding is illustrated for Au-Si and Si-Ge systems with sets of parameters for Au-Si and Au-Ge interactions chosen based on the results of DFT calculations performed for several bulk structures and small clusters. The dependences of the enthalpy of mixing in Au-Si and Au-Ge liquid alloys on the composition are calculated with the A-EAM (SW) potential and compared with experimental data. In agreement with experimental dependences, the calculated values of the enthalpy of mixing are negative in the whole range of compositions and the dependences have asymmetric shapes, with minima shifted to the Au-rich side of the alloy compositions. To further test the performance of the A-EAM (SW) potential in the description of thermodynamic properties of the alloys, the equilibrium lines on the Au-Si phase diagram are calculated based on the values of the excess chemical potential difference between Au and Si, evaluated in a series of SGCMC simulations. The Au-Si phase diagram predicted by the A-EAM potential is of the simple eutectic type with the eutectic temperature being within 50 K (8%) from the experimental value. Overall, the calculations demonstrate the ability of the A-EAM (SW) potential to capture the main characteristics of the experimental dependences and to provide an adequate semiquantitative description of the structural and thermodynamic properties of binary systems with mixed type of bonding. With clear pass existing for parameterization of cross interactions between Si/Ge and a broad range of metals, the A-EAM (SW) potential shows a

considerable promise for enabling large-scale atomistic simulations of metal-Si/Ge systems.

ACKNOWLEDGMENTS

The authors would like to thank Barend Thijsse of the Delft University of Technology and Robert A. Johnson of the University of Virginia for useful suggestions and discussions. Financial support of this work was provided by the National Science Foundation through the University of Virginia MRSEC Center for Nanoscopic Materials Design and Air Force Office of Scientific Research (Award No. FA9550-09-1-0245).

*Author to whom correspondence should be addressed; lz2n@virginia.edu

[1] M. S. Daw and M. I. Baskes, Phys. Rev. B **29**, 6443 (1984).
[2] S. M. Foiles, Phys. Rev. B **32**, 3409 (1985).
[3] R. A. Johnson, Phys. Rev. B **37**, 3924 (1988).
[4] F. H. Stillinger and T. A. Weber, Phys. Rev. B **31**, 5262 (1985).
[5] K. Ding and H. C. Andersen, Phys. Rev. B **34**, 6987 (1986).
[6] J. Tersoff, Phys. Rev. B **37**, 6991 (1988).
[7] J. Tersoff, Phys. Rev. Lett. **61**, 2879 (1988).
[8] D. W. Brenner, Phys. Rev. B **42**, 9458 (1990).
[9] D. W. Brenner, O. A. Shenderova, J. A. Harrison, S. J. Stuart, B. Ni, and S. B. Sinnot, J. Phys.: Condens. Matter **14**, 783 (2002).
[10] A. F. Voter, in *Intermetallic Compounds: Principles and Practice*, edited by J. H. Westbrook and R. L. Fleischer (Wiley, New York, 1995), Vol. 1, pp. 77–90.
[11] S. M. Foiles, M. I. Baskes, and M. S. Daw, Phys. Rev. B **33**, 7983 (1986).
[12] R. A. Johnson, Phys. Rev. B **39**, 12554 (1989).
[13] X. W. Zhou, H. N. G. Wadley, R. A. Johnson, D. J. Larson, N. Tabat, A. Cerezo, A. K. Petford-Long, G. D. W. Smith, P. H. Clifton, R. L. Martens, and T. F. Kelly, Acta Mater. **49**, 4005 (2001).
[14] H. Rafii-Tabar and A. P. Sutton, Philos. Mag. Lett. **63**, 217 (1991).
[15] M. Laradji, D. P. Landau, and B. Dünweg, Phys. Rev. B **51**, 4894 (1995).
[16] J. Tersoff, Phys. Rev. B **39**, 5566 (1989).
[17] M. I. Baskes, Phys. Rev. B **46**, 2727 (1992).
[18] M. I. Baskes, Mater. Sci. Eng. A **261**, 165 (1999).
[19] C.-L. Kuo and P. Clancy, Surf. Sci. **551**, 39 (2004).
[20] A. Noreyan, Y. Qi, and V. Stoilov, Acta Mater. **56**, 3461 (2008).
[21] H. P. Wang and B. Wei, J. Phys. D **42**, 035414 (2009).
[22] C.-L. Kuo and P. Clancy, Modell. Simul. Mater. Sci. Eng. **13**, 1309 (2005).
[23] Z.-Y. Zhang, Y.-T. Lu, and H. Metiu, Surf. Sci. Lett. **248**, L250 (1991).
[24] K. Mae, Thin Solid Films **395**, 235 (2001).
[25] B. J. Thijsse, Nucl. Instrum. Methods Phys. Res. B **228**, 198 (2005).
[26] K. Albe, K. Nordlund, and R. S. Averback, Phys. Rev. B **65**, 195124 (2002).
[27] D. W. Brenner, Phys. Rev. Lett. **63**, 1022 (1989).
[28] B. J. Thijsse, Phys. Rev. B **65**, 195207 (2002).
[29] A. M. Dongare, L. V. Zhigilei, A. M. Rajendran, and B. LaMattina, Composites, Part B **40**, 461 (2009).
[30] W. Yu, Z. Q. Wang, and D. Stroud, Phys. Rev. B **54**, 13946 (1996).
[31] P. C. L. Stephenson, M. W. Radny, and P. V. Smith, Surf. Sci. **366**, 177 (1996).
[32] S. J. Cook and P. Clancy, Phys. Rev. B **47**, 7686 (1993).
[33] H. Balamane, T. Halicioglu, and W. A. Tiller, Phys. Rev. B **46**, 2250 (1992).
[34] *CRC Handbook of Chemistry and Physics*, edited by D. R. Lide (CRC, Ann Arbor, 1991).
[35] B. Predel, in *Phase Equilibria, Crystallographic and Thermodynamic Data of Binary Alloys*, Landolt-Börnstein, New Series, Group IV, Vol. 5, edited by O. Madelung (Springer-Verlag, Berlin, 1991), and references therein.
[36] T. Nakayama, S. Itaya, and D. Murayama, J. Phys.: Conf. Ser. **38**, 216 (2006).
[37] G. Kresse and J. Hafner, J. Phys.: Condens. Matter **6**, 8245 (1994).
[38] J. P. Perdew and Y. Wang, Phys. Rev. B **45**, 13244 (1992).
[39] D. Vanderbilt, Phys. Rev. B **41**, 7892 (1990).
[40] F. Birch, Phys. Rev. **71**, 809 (1947).
[41] M. J. Mehl, B. M. Klein, and D. A. Papaconstantopoulos, in *Intermetallic Compounds: Principles and Applications*, edited by J. H. Westbrook and R. L. Fleischer (Wiley, London, 1994), Vol. 1, pp. 195–210.
[42] I. H. Lee and R. M. Martin, Phys. Rev. B **56**, 7197 (1997).
[43] R. T. DeHoff, *Thermodynamics in Material Science* (McGraw-Hill, New York, 1992).
[44] S. E. Wood, J. Chem. Phys. **15**, 358 (1947).
[45] F. Sommer, R. N. Singh, and V. Witusiewicz, J. Alloys Compd. **325**, 118 (2001).
[46] The entropy of mixing evaluated for liquid Au-Si alloy at 1500 K using semi-grand canonical ensemble Monte Carlo simulations is found to exceed the ideal entropy of mixing by as much as a factor of 3 at $X_{Si}=0.5$.
[47] D. Frenkel and B. Smit, *Understanding Molecular Simulation*, 2nd ed. (Academic Press, San Diego and London, 2002).
[48] D. A. Kofke and E. D. Glandt, Mol. Phys. **64**, 1105 (1988).
[49] M. Yu. Lavrentiev, R. Drautz, D. Nguyen-Manh, T. P. C. Klaver, and S. L. Dudarev, Phys. Rev. B **75**, 014208 (2007).
[50] P. L. Williams, Y. Mishin, and J. C. Hamilton, Modell. Simul. Mater. Sci. Eng. **14**, 817 (2006).
[51] P. C. Kelires and J. Tersoff, Phys. Rev. Lett. **63**, 1164 (1989).
[52] D. S. Ivanov and L. V. Zhigilei, Phys. Rev. B **68**, 064114 (2003).
[53] D. Buta, M. Asta, and J. J. Hoyt, J. Chem. Phys. **127**, 074703 (2007).